Research Square

Preprints are preliminary reports that have not undergone peer review.
They should not be considered conclusive, used to inform clinical practice,
or referenced by the media as validated information.

Synthesis of Al-Doped SBA-15, MCM-41, MCM-48 by Incorporation and Catalytic Performance in Propylene oligomerization

Mihai Ion POSTELNICU
Petroleum-Gas University of Ploiesti
Diana Luciana CURSARU
dianapetre@upg-ploiesti.ro

Petroleum-Gas University of Ploiesti
Dănuța MATEI
Petroleum-Gas University of Ploiesti
Sonia MIHAI
Petroleum-Gas University of Ploiesti

Research Article

Keywords: Al-SBA-15, Al-MCM-41, Al-MCM-48, incorporation, oligomerization, propylene

Posted Date: April 9th, 2026

DOI: https://doi.org/10.21203/rs.3.rs-9232415/v1

License: This work is licensed under a Creative Commons Attribution 4.0 International License.
Read Full License

Additional Declarations: No competing interests reported.

Synthesis of Al-Doped SBA-15, MCM-41, MCM-48 by Incorporation and Catalytic Performance in Propylene oligomerization

Mihai Ion POSTELNICU, Diana Luciana CURSARU*, Dănuța MATEI, Sonia MIHAI,

Faculty of Petroleum Refining and Petrochemistry, Petroleum-Gas University of Ploiesti, 100680 Ploiești, Romania;

*Corresponding author: dianapetre@upg-ploiesti.ro;

Contributing authors: danuta.matei@upg-ploiesti.ro (D.M.), smihai@upg-ploiesti.ro (S.M.), mihai_ion.postelnicu@yahoo.com (M.P.)

Abstract

Aluminum-doped mesoporous silica materials SBA-15, MCM-41, and MCM-48 were synthesized by direct incorporation and then investigated for gas-phase oligomerization of propylene at temperatures 433-503K and 5 atm pressure. The synthesis method aimed to create aluminum-based active centers suitable for catalytic processes. The resulting samples were characterized using X-ray diffraction (XRD), nitrogen adsorption–desorption (BET), Fourier transform infrared spectroscopy (FTIR), and scanning electron microscopy (SEM). Results indicated that aluminum incorporated during synthesis is homogeneously distributed within the silica framework, and the synthesized materials possess unique structural characteristics, including a large specific surface area, high pore volume, and tunable pore sizes within the mesoporous range of 2 to 50 nm. Catalytic tests showed that propylene conversion and productivity increase with temperature following Arrhenius behavior (Ea, app = 39 – 55 kJ/mol), while flow rate experiments indicated negligible external diffusion limitations. Time-on-stream analysis revealed progressive deactivation due to pore blocking by heavier oligomers. Among the studied catalysts, Al-SBA-15 exhibited the highest conversion, superior selectivity toward heavier products (C10-C12+) and improved stability, highlighting the critical role of pore size and connectivity in controlling activity and selectivity during propylene oligomerization.

Keywords: Al-SBA-15; Al-MCM-41; Al-MCM-48; incorporation; oligomerization; propylene.

1. Introduction

Catalytic materials play an important role in industrial processes, providing efficient methods for transforming raw materials into valuable products. Among the various types of catalysts, mesoporous materials, particularly those based on silica and alumina, are gaining a lot of interest as they possess a large number of exceptional properties, such as high thermal stability with the capability of having a high surface area and adjustable pore design. MCM-41 materials containing aluminum, which include Al-MCM-41, Al-MCM-48, and Al-SBA-15, are inexpensive and have the capability of advanced biomass conversion, hydrotreatment, isomerization, adsorption, and many other catalytic applications. The processes are feasible because of their well-defined mesostructural arrangement, large pore capacity, and the presence of active metal sites. Additionally, the incorporation of aluminum into the silica framework introduces Brønsted and Lewis acid sites, which significantly enhance their catalytic activity [1-10].

The method of synthesis is one of the aspects that greatly influences the texture and the surface characteristics of the materials. Mesoporous silica materials are usually prepared by the use of templating materials, while aluminum is added using the hydrothermal method, sol-gel, impregnation, or direct incorporation. These methods enable the tailoring of pore size, surface acidity, and general mesostructural compliance to specific needs [11-13]. For example, it is possible to obtain highly ordered mesoporous structures with large surface areas by hydrothermal synthesis [14], whereas direct incorporation more often yields a uniform distribution of aluminum in silica matrix, which improves the stability and catalytic activity of the material [15-18].

Incorporation of aluminum into the silica matrix is especially useful in relation to catalytic processes since it changes the textural properties such as pore size, volume, surface area, and surface acidity. The ratio Si/Al is critical in determining these properties as it decides how much aluminum is present and in what amounts and whether the resulting material has good acidity and high catalytic activity [19, 20]. According to Locus R. et al., alkaline activation of Al-MCM-41 via 0.05 M NaOH results in an effective acidic material due to the transformation of octahedral Al into tetrahedral accessible Al and incorporating formerly inaccessible Al from the pore walls towards the surface. The process also facilitates the formation of interconnected mesopores with an estimated size between 3 and 12 nm while retaining particle structure. This process further fourfold the catalytic activity of the particle, especially in conducting acid-catalyzed reactions such as the alkylation of toluene [7].

The structural characteristics of Al-MCM-41, Al-MCM-48, and Al-SBA-15 are also influenced by diverse synthesis techniques. These materials are dissimilar in terms of pore symmetry and pore size, thus

altering the distribution of active sites as well as the resultant catalytic performance. As an instance, Sari Yilmaz M. et al. synthesized MCM-41 by classical and ultrasound methods, finding that the ultrasound method created lower surface area materials than expected. The Sr^{2+} adsorption on MCM-41 was pH dependent, where the most Sr^{2+} ions were adsorbed at a pH of 5, while the material had pseudo-second-order kinetics. This phenomenon makes it clear how suitable the material is for aqueous ion removal applications [21]. As previously stated, Prabhu A. et al. demonstrated that Al-SBA-15 catalysts formed using ultrasonic procedures are superior to those formed via hydrothermal techniques. These catalysts achieved 70% ethylbenzene conversion and 82% para-tert-butylethylbenzene selectivity. This remarkable achievement was made possible due to the higher aluminium incorporation along with improved mesoporous structure. This study focuses on the critical role that synthesis methods play in customizing mesoporous materials for specific catalytic and adsorption applications as well [18].

This study examines how incorporating aluminum either during material formation or through post-synthetic modification influences the structural and textural features of mesoporous silicas, specifically MCM-41, MCM-48, and SBA-15, with an aluminum content of 3 wt. %. The samples were produced via a sol-gel route and evaluated using several analytical tools, including FTIR spectroscopy, XRD, SEM coupled with EDS, nitrogen sorption measurements (BET), and thermogravimetric analysis. The results demonstrate that the selected preparation pathway significantly influences the final material properties. Additionally, the study examines how the resulting textural and morphological characteristics affect catalytic performance in the gas-phase oligomerization of propene, showing that pore architecture plays a decisive role in determining activity, selectivity towards heavier oligomers, and catalyst stability under reaction conditions. Beyond comparative materials characterization, this study provides valuable mechanistic insight into how aluminum incorporation and mesopore topology jointly govern activity, product distribution and deactivation, thereby offering a robust foundation for the development of next-generation catalyst for propylene oligomerization.

2. Experimental

2.1. Materials and Reagents

Al-MCM-41 and Al-MCM-48 molecular sieves were synthesized using tetraethyl orthosilicate (TEOS, 99%) as the silica source, cetyltrimethylammonium bromide (CTAB, 99%) as the structure-directing agent, absolute ethanol (99.5%), ammonium hydroxide (NH_4OH, 29% w/w), and deionized water. All chemicals were obtained from Sigma-Aldrich Chemical Co. For Al-SBA-15 synthesis, tetraethyl orthosilicate (99%), the triblock copolymer PEG-PPG-PEG (Pluronic P123; Mw ~ 5800), hydrochloric acid (HCl, 35%),

and deionized water were used, also sourced from Sigma-Aldrich Chemical Co. Aluminum chloride ($AlCl_3 \cdot 6H_2O$) was purchased from Carl Roth GmbH.

2.2. Synthesis of Al-doped molecular sieves

Al-doped MCM-41, MCM-48, and SBA-14 were prepared following a method documented in the literature, which was also utilized in our earlier studies regarding various applications of these molecular sieves [22-27]. The aluminum precursor employed was $AlCl_3 \cdot 6H_2O$. A solution was made by dissolving 6 g of the compound in distilled water, which was then utilized in the synthesis processes similar to those carried out in our previous study involving Ni as metal on mesoporous silicas [27]. All the procedure steps were the same as reported before. The percent of aluminum incorporated in the silicas was 3%.

2.3.Characterization techniques

The synthesized materials' structural and chemical properties were assessed using powder X-ray diffraction (XRD) conducted with a Bruker D8 Advance diffractometer (Karlsruhe, Germany) set up in θ–θ geometry. Measurements took place using Cu Kα radiation (λ = 1.5418Å) at 40 kV operating voltage and a current of 40 mA. The diffraction spectra obtained were employed to evaluate the crystallographic phases, extent of structural order, and elemental composition of the samples.

Textural characteristics, such as specific surface area, pore volume, and pore size distribution, were assessed through nitrogen adsorption–desorption experiments at 77 K, conducted using a Quantachrome Nova 2200e analyzer (Quantachrome Instruments, Boynton Beach, FL, USA). Before measurements, samples were subjected to degassing in a vacuum at 150 °C for 3 hours. The Brunauer–Emmett–Teller (BET) theory was utilized in the relative pressure range of $0.05 \leq p/p_o \leq 0.30$ to determine surface areas, while pore size distributions were obtained using the Barrett–Joyner–Halenda (BJH) method applied to the adsorption branch of the isotherms. Data were analyzed using NovaWin software (Quantachrome, Boca Raton, FL, USA)

Thermal properties and stability were evaluated via thermogravimetric (TGA) and differential thermogravimetric (DTG) analyses conducted with a Setaram Labsys Evo S60/58986 device (USA). The analyses were conducted in an argon atmosphere ranging from 30 to 800 °C, maintaining a steady heating rate of 10 °C/min.

The materials' morphology and particle characteristics were analyzed using scanning electron microscopy (SEM) with a Thermo Fisher Scios 2 HiVac Dual-Beam FIB-SEM system (Brno, Czech Republic), which provides high-resolution imaging to investigate particle shape, size, and surface texture.

Fourier transform infrared (FT-IR) spectroscopy was conducted using a Shimadzu IRTracer-100 device (Kyoto, Japan) across the spectral range of 400–4000 cm^{-1}. This evaluation allowed for the identification of functional groups and confirmation of the silica frameworks' stability.

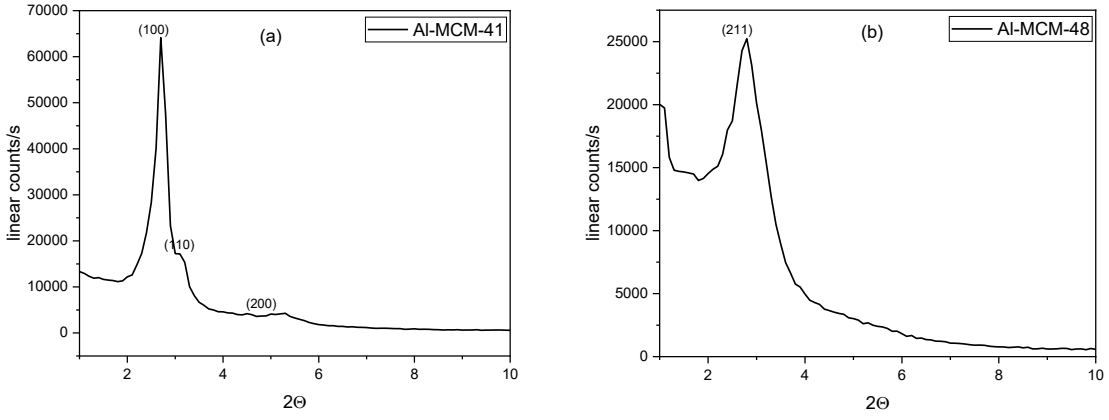
The products obtained during propylene oligomerization were analyzed by GC/MS and GC/FID. GC/MS spectra were recorded with a 7890A Agilent with the NIST Library database for compound identification with a DSQ mass detector. *GC Method:* Column HP-5 MS (L=30m, D=250 µm, d=0.25 µm); Oven Program: 40ºC (hold 1 min), then 10ºC/min to 220ºC (hold 1 min); Carrier gas: He, Flow=1ml/min, Injector Temp.: 200ºC; Injection Volume: 1 µl; split 1:10. *MS Method:* QQQ Collision Cell: Quench Flow Gas (He) = 2.2 ml/min; Collision Flow Gas (N_2) = 1.5 ml/min; Type of Source: EI; Electron Energy: 70eV; Source Temp.: 230ºC, Aux Temp.: 240ºC; Scan Segment: 40-400; Type of Chromatogram: TIC

GC/FID spectra were recorded with a Varian CP-3800 GC. *GC Method:* Column DB-5 (L=30m, D=250 µm, d=0.25 µm); Oven Program: 90ºC (hold 1 min), then 10ºC/min to 220ºC (hold 1 min); Carrier gas: He, Flow=1mL/min, Injector Type: CP-1177 Liquid Injector; Injector Temp.: 200ºC; Injection Volume: 1 µl; Injector Split Mode: split 1:10; *FID Method:* Detector temp: 300ºC; Make-up Flow: 25 ml/min; H_2 Flow: 30 ml/min; Air Flow: 300 ml/min.

3. Results and Discussion

3.1. X-ray diffraction (XRD)

The low-angle X-ray diffraction (XRD) patterns and the crystallite size of the synthesized Al-doped mesoporous molecular sieves MCM-41, MCM-48, and SBA-15 are presented in Figure 1. Al-MCM-41 showed three characteristic peaks at 2θ = 2.64°, 3.10°, and 5.15° corresponding to the Miller indices (100), (110), and (200) (Figure 1a).



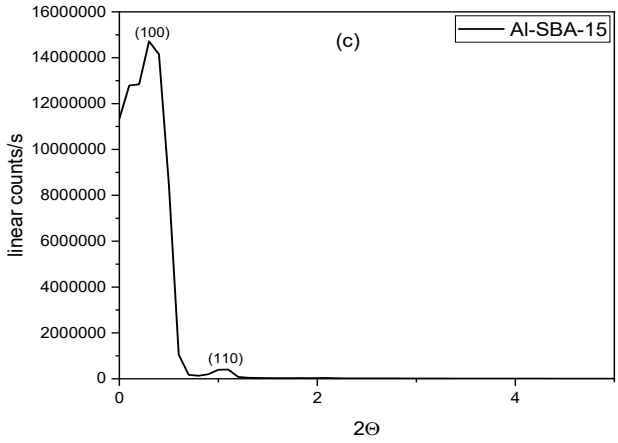


Fig.1. Low-angle XRD patterns of (a) Al-MCM-4, (b) Al-MCM-48 and (c) Al-SBA-15

The presence of three peaks for Al-MCM-41 indicates a highly ordered mesoporous structure with a hexagonal pore array. Al-MCM-48 samples (Figure 1b) display one diffraction peak corresponding to (211) reflections. The presence of only this peak indicates a partial or complete loss of long-range mesostructural order, often associated with a collapse or distortion of its original cubic Ia3d symmetry. This behavior often results from framework modification with aluminum or post-synthesis treatments, which reduce the contrast between the pore walls and voids, leading to a poorly ordered or partially degraded mesoporous structure.

SBA-15 presents two distinctive peaks: a prominent peak at 2θ = 0.305° and a weak peak at 2θ = 1.03°. These peaks correspond to the (100) and (110) reflections, respectively, as illustrated in Figure 1c.

To further characterize the structural features, the Scherrer equation (1), was applied to estimate the size of ordered mesostructural domains. It is important to note that, in the case of mesoporous materials, the low-angle diffraction peaks arise from pore ordering rather than atomic-scale crystallinity. Therefore, the calculated values should be interpreted as an approximate measure of the coherence length of the mesostructural ordering rather than true crystallite sizes. The Scherrer equation is given by:

$$LC = \frac{K \cdot \lambda}{\beta \cdot \cos\theta} \qquad (1)$$

where:

LC is the mean size of the crystallites (nm),

K is the shape factor equal to 0.94,

λ is the wavelength of the X-rays (1.54Å),

θ is the Bragg angle (°),

β is the line broadening at half the maximum intensity peak (FWHM) in radians.

Table 1 displays the low angle XRD peak parameters and estimated mesostructural domain sizes of Al-Based molecular sieves.

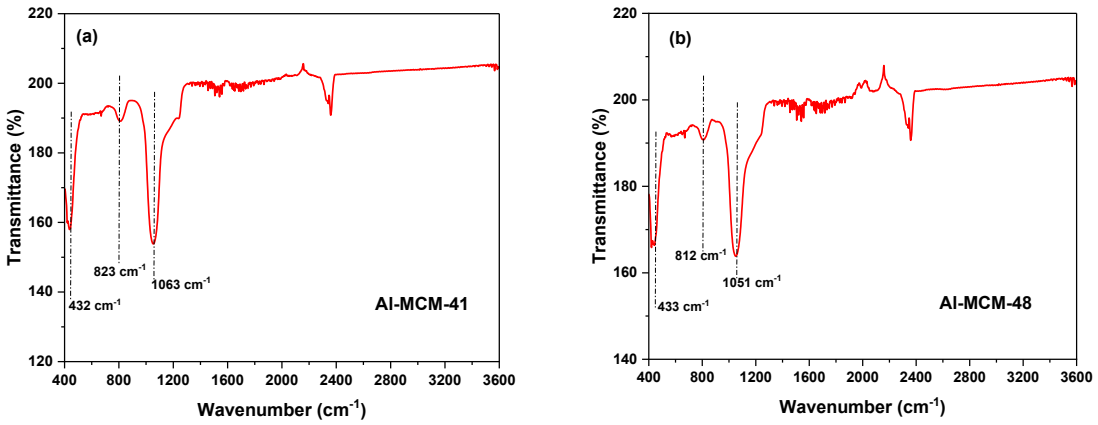
Table 1. Low-angle XRD peak parameters and estimated mesostructural domain sizes of Al-based molecular sieves

Samples	Peak 1			Peak 2			$\overline{LC}$
	2θ	*FWHM*	*LC*	2θ	*FWHM*	*LC*	
Al-MCM-41	2.7	0.427	3.25	-	-	-	3.25
Al-MCM-48	2.78	0.228	6.43	-	-	-	6.43
Al-SBA-15	0.326	0.388	3.73	1.06	0.2	7.25	5.46

These values should be considered comparative rather than absolute, as the Scherrer approach provides only an approximate estimation for mesostructured materials.

3.2. FT-IR investigations

Figure 2 shows the FT-IR spectra for Al-MCM-14, Al-MCM-48, and Al-SBA-15 in the wavenumber range of 4000 cm^{-1} to 400 cm^{-1}. Following modification with aluminum, the FT-IR spectra of Al-MCM-41, Al-MCM-48, and Al-SBA-15 retained the same main silica absorption bands, indicating that neither the incorporation nor the impregnation of aluminum significantly altered the silica framework. This result is consistent with the one obtained in the previous work for Ni-molecular sieves [27]. However, a band near 1244 cm^{-1} assigned to Si–O–Al vibrations suggests successful substitution of Si^{4+} by Al^{3+} in the silica network.



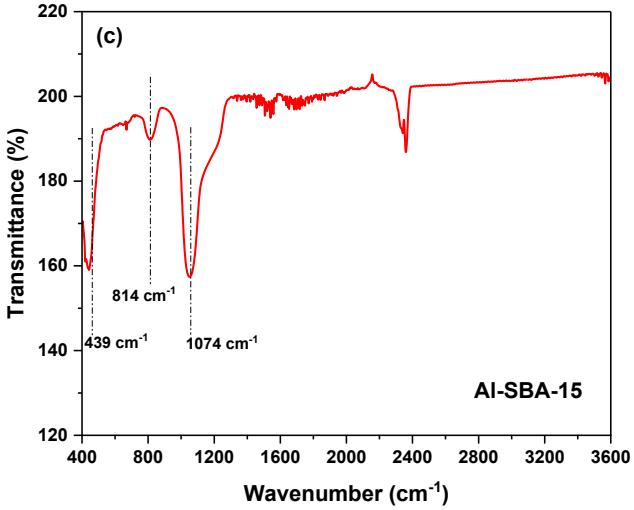
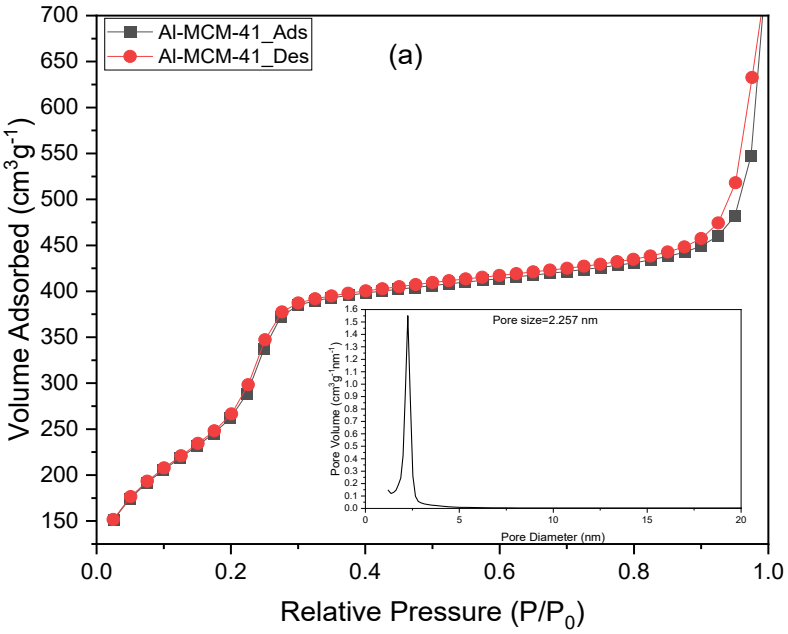
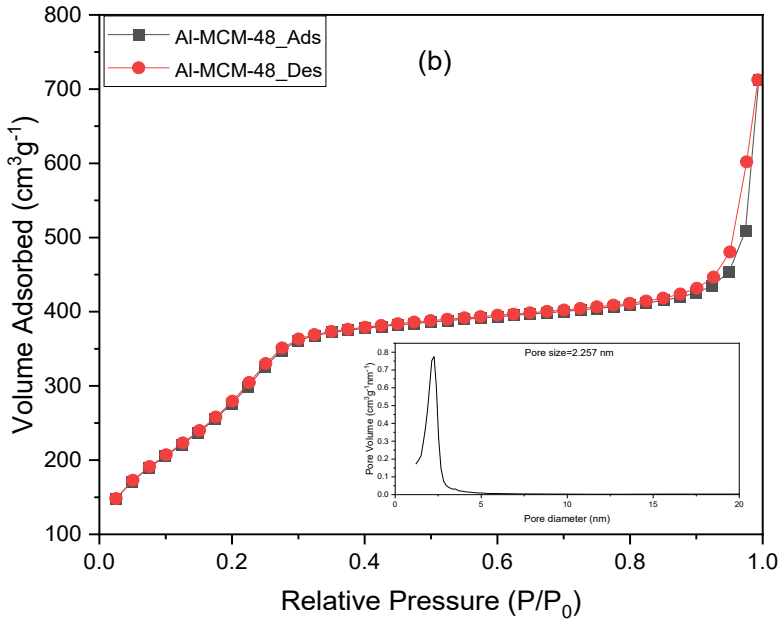


Fig. 2. FT-IR spectra of (a) Al-MCM-41, (b) Al-MCM-48 and (c) Al-SBA-15

3.3. N_2 adsorption-desorption

The nitrogen adsorption/desorption isotherms of all Al-doped molecular sieves are presented in Figure 3. After aluminum loading into the molecular sieves, the nitrogen adsorption–desorption isotherms for Al-MCM-41 (Figure 3a), Al-MCM-48 (Figure 3b), and Al-SBA-15 (Figure 3c) maintain a type IV profile. A sharp increase in the volume of adsorbed nitrogen is observed at relative pressures (P/P_0) between 0.2 and 0.4, indicating the presence of a highly uniform mesoporous structure. The H1-type hysteresis loop between the adsorption and desorption branches further suggests cylindrical pore geometry and a narrow pore size distribution. The pore size distribution exhibits a pronounced maximum in the 3–4 nm range, confirming the uniformity of the pore system.


Al-MCM-41_Ads
Al-MCM-41_Des
(a)
Volume Adsorbed (cm3g-1)
Relative Pressure (P/P0)
Pore size=2.257 nm
Pore Volume (cm3g-1nm-1)
Pore Diameter (nm)


Al-MCM-48_Ads
Al-MCM-48_Des
(b)
Volume Adsorbed (cm3g-1)
Relative Pressure (P/P0)
Pore size=2.257 nm
Pore Volume (cm3g-1nm-1)
Pore diameter (nm)

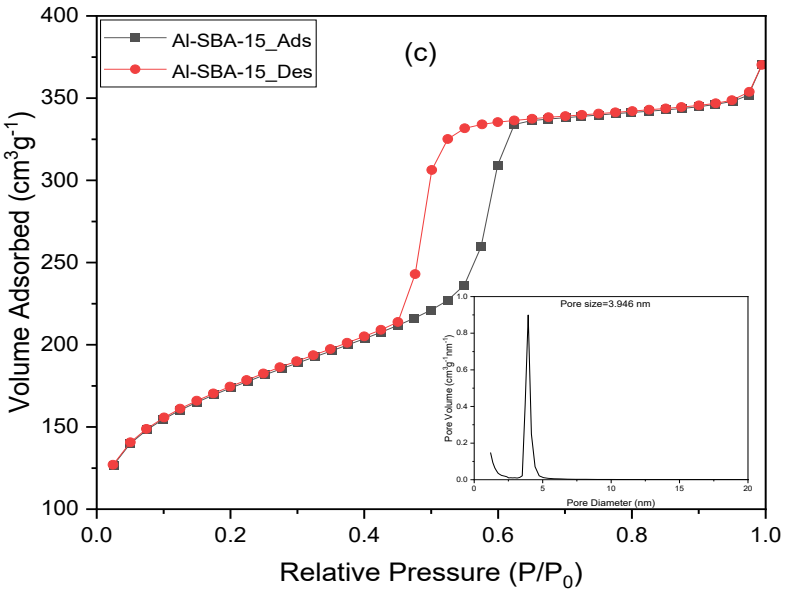


Fig. 3. N_2 adsorption-desorption isotherms of (a) Al-MCM-41, (b) Al-MCM-48 and (c) Al-SBA-15 and BHJ pore size distribution curves (insets)

For the Al-MCM-48 sample, the nitrogen adsorption isotherm exhibits the characteristics of a type IV isotherm, typical of mesoporous materials. A gradual increase in the adsorbed nitrogen volume is observed at relative pressures (P/P_0) between 0.2 and 0.4, followed by a less pronounced inflection compared to Al-MCM-41. This behavior reflects the cubic, three-dimensional pore structure of MCM-48. The presence of an H2-type hysteresis loop is indicative of a complex, interconnected pore network. The pore size distribution reveals a well-defined peak around 3 nm, confirming the uniformity of the three-dimensional mesoporous framework.

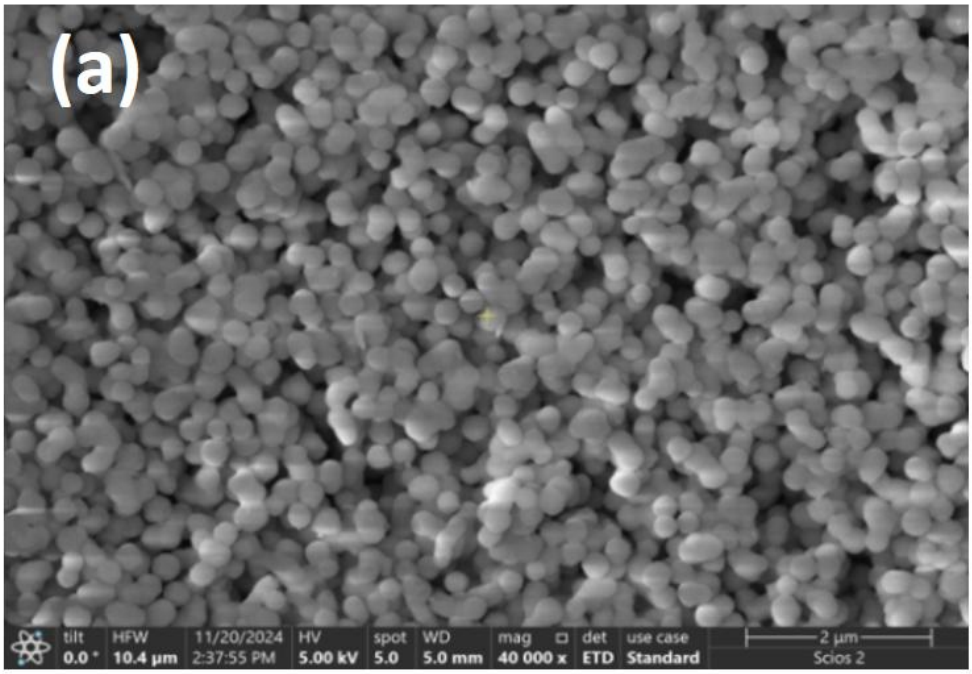
For the Al-SBA-15 sample, the nitrogen adsorption isotherm exhibits the characteristic features of a type IV isotherm. A sharp increase in the volume of adsorbed nitrogen is observed at higher relative pressures (P/P_0 = 0.6–0.8) compared to Al-MCM-41 and Al-MCM-48, reflecting the presence of larger pore sizes. The pronounced H1-type hysteresis loop is indicative of cylindrical pores with uniform dimensions and open channels. The pore size distribution confirms this, showing a well-defined peak in the 6–7 nm range, which is characteristic of the large, ordered mesopores typical of SBA-15. In table 2 are presented the pore diameter, pore volume and surface area for the synthesized samples.

Table 2. Pore diameter, pore volume and surface area of Al-MCM-41, Al-MCM-48 and Al-SBA-15

Sample	S_{BET} (m^2/g)	Dp (nm)	Vp (cm^3g^{-1})
Al-MCM-41	1437	2.26	1.25
Al-MCM-48	1454	2.26	0.83
Al-SBA-15	630	3.95	0.85

3.4. SEM-EDS investigations

SEM images of the Al-incorporated MCM-41 material (Figure 4a) show a collection of particles with submicron dimensions and spherical shape. Their relatively uniform distribution and characteristic surface texture confirm the successful synthesis of the aluminum-modified MCM-41 mesoporous material.



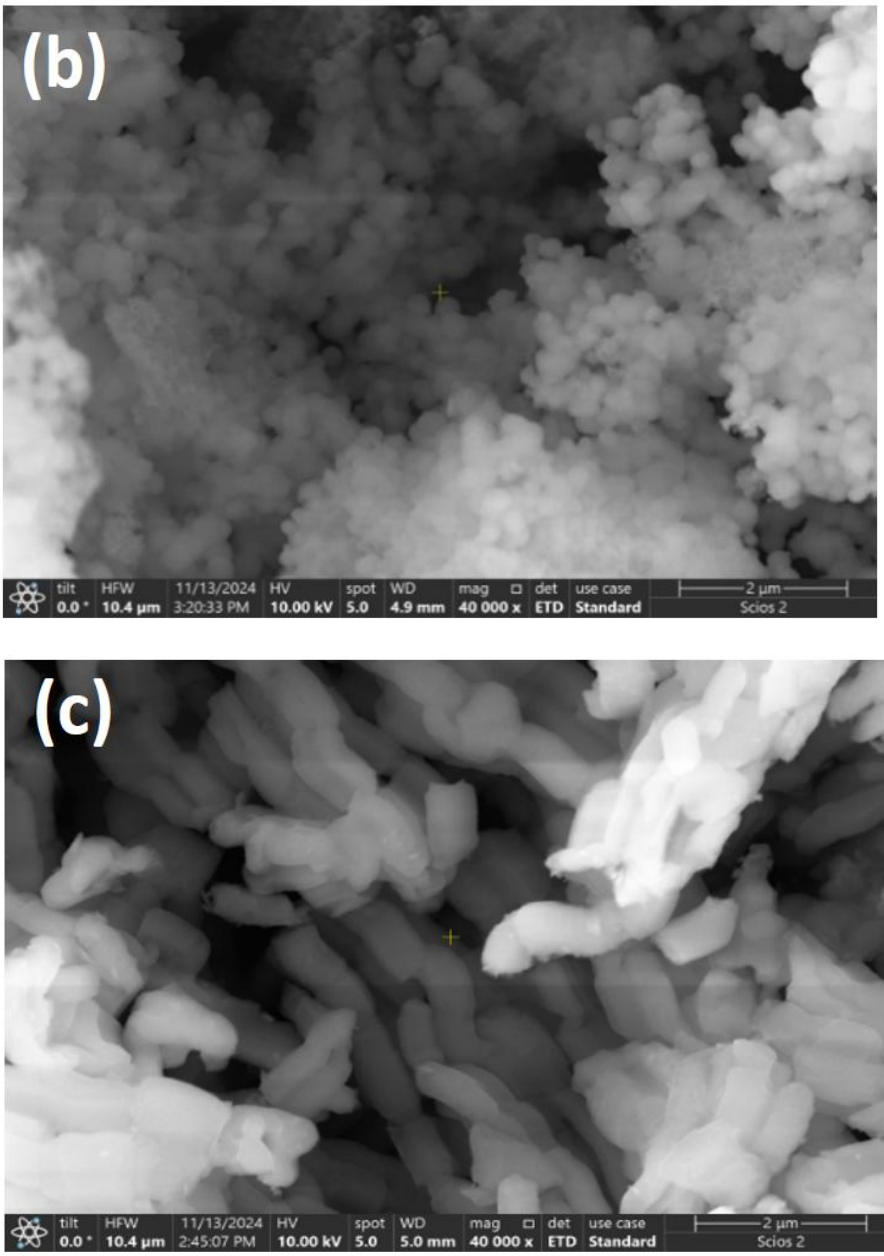


Fig. 4. SEM images of (a) Al-MCM-41, (b) Al-MCM-48 and (c) Al-SBA-15

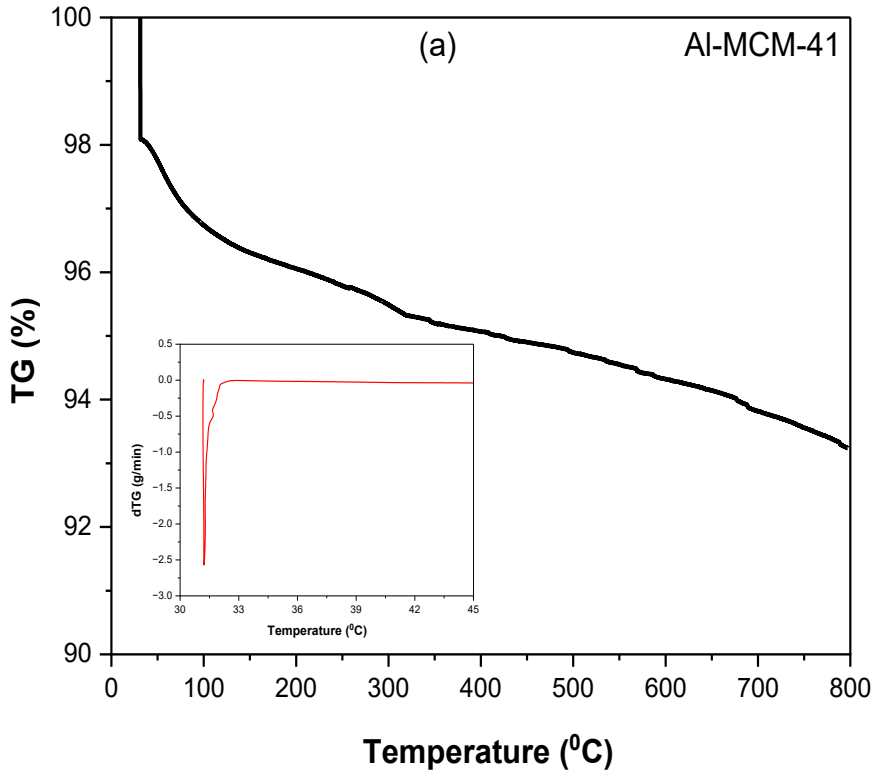
The Al-incorporated MCM-48 sample (Figure 4b) exhibits a relatively uniform morphology, characterized by submicron-sized particles and a homogeneous distribution of agglomerates.

For the Al-incorporated SBA-15 sample (Figure 4c), SEM images reveal a structure composed of particles with uniform morphology, forming compact agglomerates of relatively homogeneous size. The surface texture indicates the preservation of the characteristic structural features of SBA-15-type materials, suggesting the effective incorporation of aluminum into the mesoporous framework.

3.5. Thermogravimetric analysis with Derivative Thermogravimetry (TGA-dTG)

The TGA curve of the Al-incorporated MCM-41 sample (Figure 5a) displays a gradual mass loss occurring in several stages. The initial mass loss below approximately 100 °C corresponds to desorption of physically adsorbed water. A second mass-loss region appears between approximately 200 and 600 °C and is associated with the removal of surface hydroxyl groups. The corresponding DTA signals exhibit endothermic features. Above approximately 600°C, only minor weight changes occur, indicating that the material maintains its structural integrity at elevated temperatures.

The TGA curve of the Al-incorporated MCM-48 sample (Figure 5b) reveals a multi-step thermal degradation process. The first step, occurring up to approximately 100 °C, corresponds to the removal of physisorbed water. This is followed by a gradual mass loss in the 200–600 °C range, which is attributed to surface dihydroxylation. The associated DTA curve confirms the endothermic nature of these transformations, and the minimal mass loss at higher temperatures suggests the material possesses a stable framework and thermally stable structure.



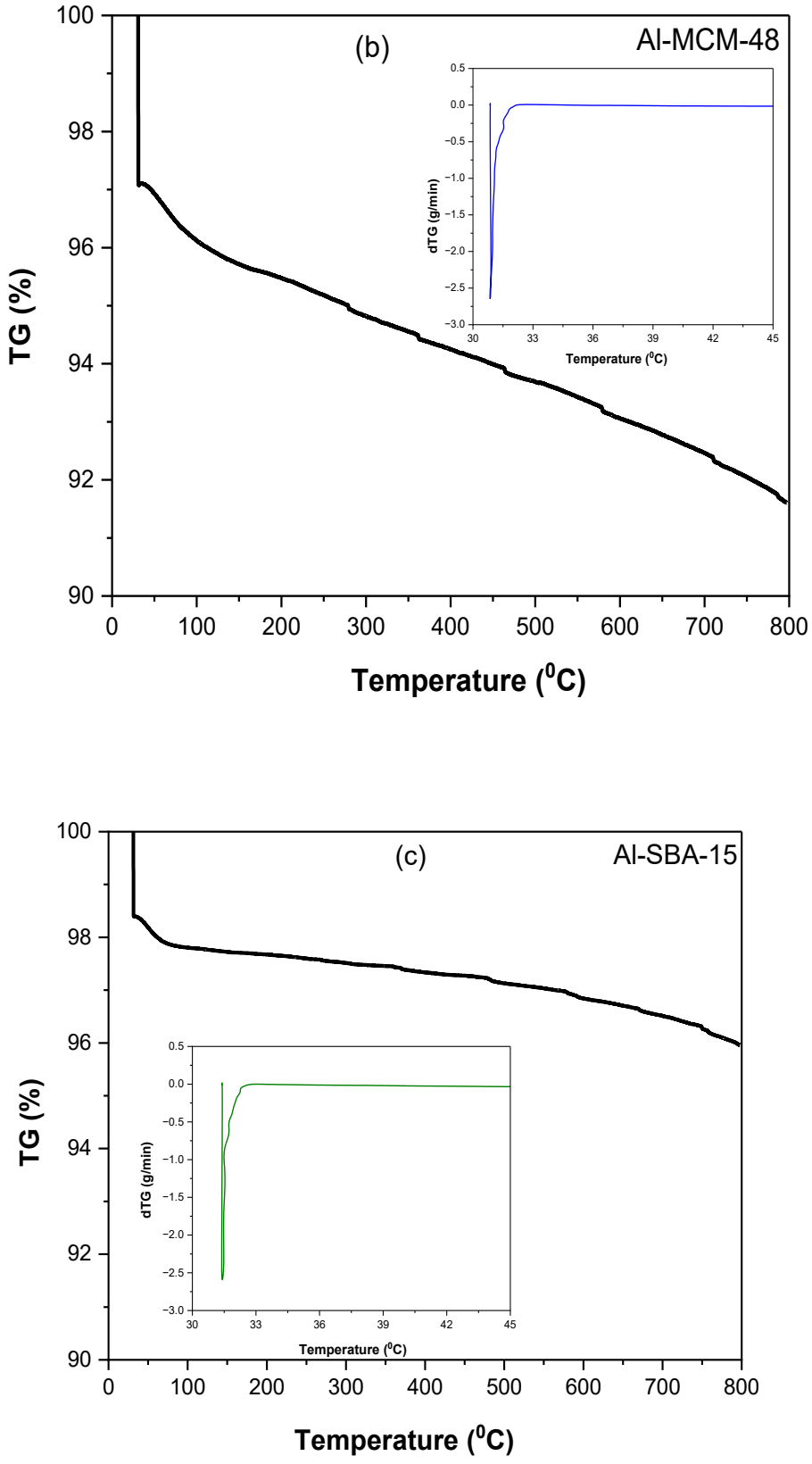


Fig. 5. TGA and dTG (insets) thermograms of (a) Al-MCM-41, (b) Al-MCM-48 and (c) Al-SBA-15

The TGA curve of the Al-incorporated SBA-15 sample (Figure 5c) reveals a multi-stage thermal degradation process. The first mass loss, occurring up to approximately 150 °C, corresponds to the removal of physisorbed water from the mesoporous structure. This is followed by a moderate mass loss in the 200–600 °C range, attributed to the surface dihydroxylation process. The accompanying DTA curve confirms the endothermic nature of these transformations. The minimal mass loss at higher temperatures indicates the high thermal stability and robust framework of the material.

A comprehensive characterization of an industrial catalyst used in olefin oligomerization was performed using the same techniques as for the synthesized ones. These analyzes were aimed at elucidating the structural disorder, mesoporosity and surface functionalities governing catalytic behavior.

The wide-angle XRD patterns (figure 6) does not show distinct diffraction peaks, displaying instead a low and nearly constant intensity, indicating that the catalyst is predominantly amorphous or very poorly crystalline. The support is most likely amorphous silica or poorly ordered γ-Al2O3, commonly used in industrial oligomerization catalysts.

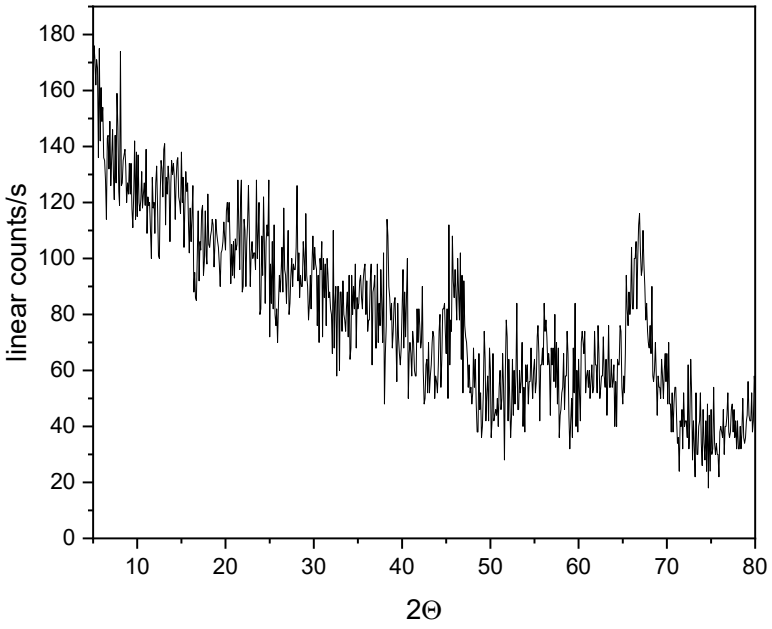


Fig. 6. XRD pattern for industrial oligomerization catalyst

The absence of diffraction peaks corresponding to metallic phases suggest that the active species are highly dispersed or present as amorphous oxides which favor catalytic activity and selectivity in olefin oligomerization.

Moving forward, the N2 adsorption-desorption isotherm (figure 7) corresponds to type IV (IUPAC), characteristic of mesoporous materials. A pronounced adsorption step at P/P0 = 0.6 – 0.8 and a plateau at high relative pressures are observed.

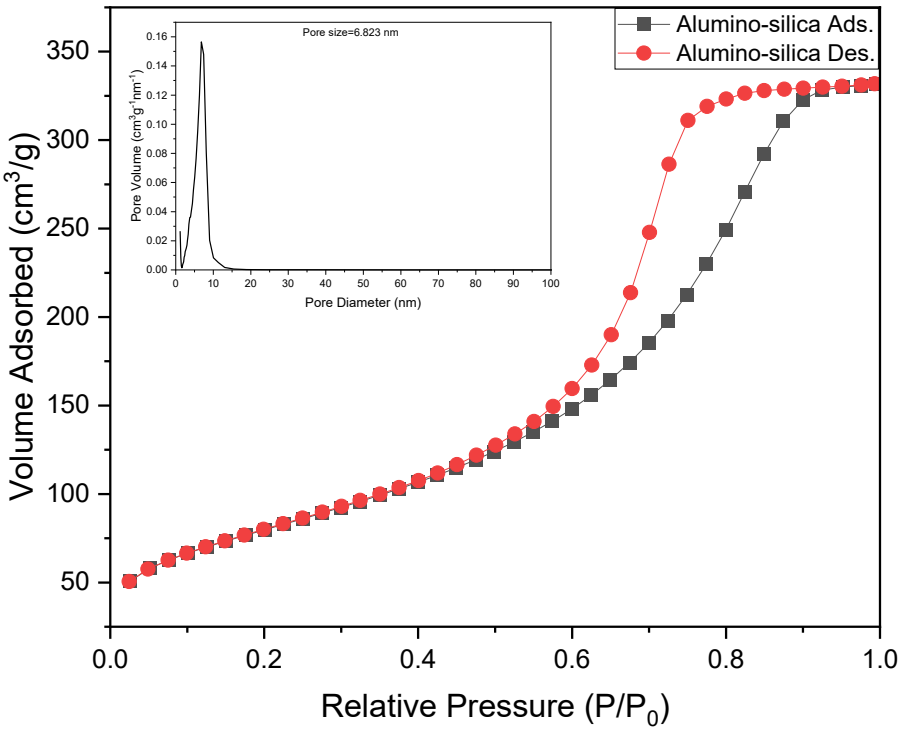


Fig. 7. N2 adsorption-desorption isotherms of industrial oligomerization catalyst and pore size distribution curves (insets)

The hysteresis loop is of type H2, indicating disordered mesoporosity with a broad pore size distribution. The pore size distribution is centered in the mesoporous range (5-20 nm), suggesting a high specific surface area (~250-400 m2/g) and a significant pore volume (~0.4-0.6 cm3/g). These properties ensure good accessibility and diffusion of reactants.

The TGA analysis (figure 8) shows two main weight loss regions. The first (30-150°C, ~ 1-2%) corresponds to the removal of physically adsorbed water. The second (150-800°C, ~2-5%) is attributed to gradual dehydroxylation of surface –OH groups. The absence of significant mass loss events indicates that the catalyst is free of organic residues and thermally stable.

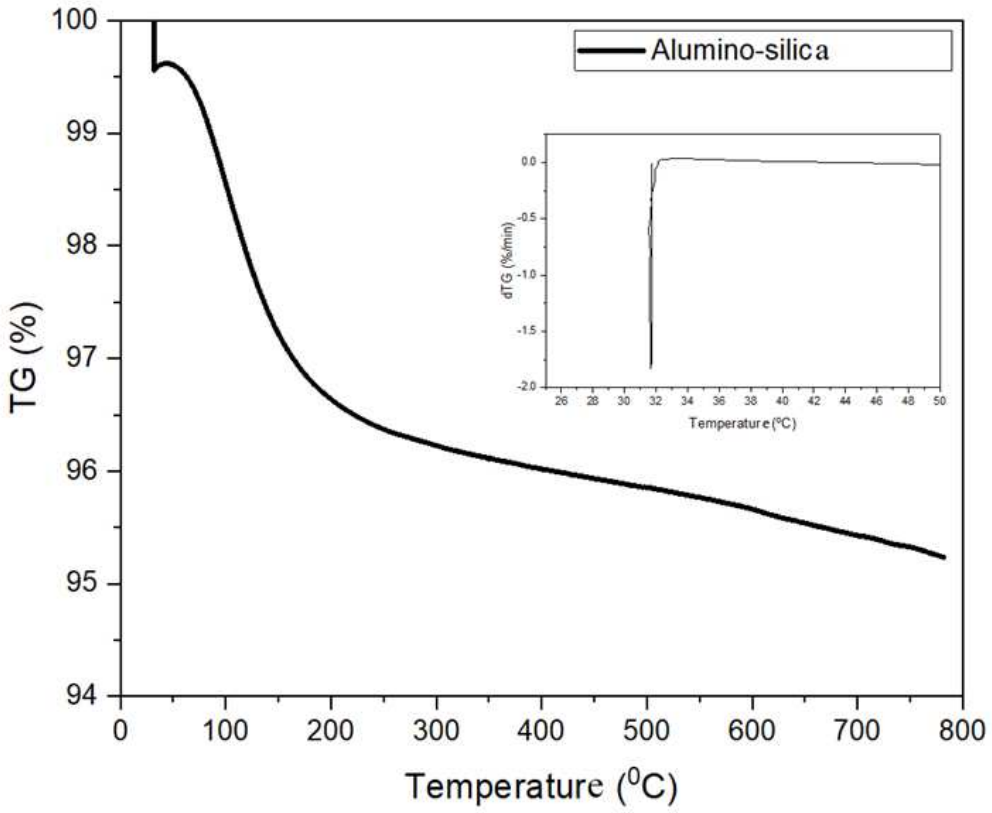
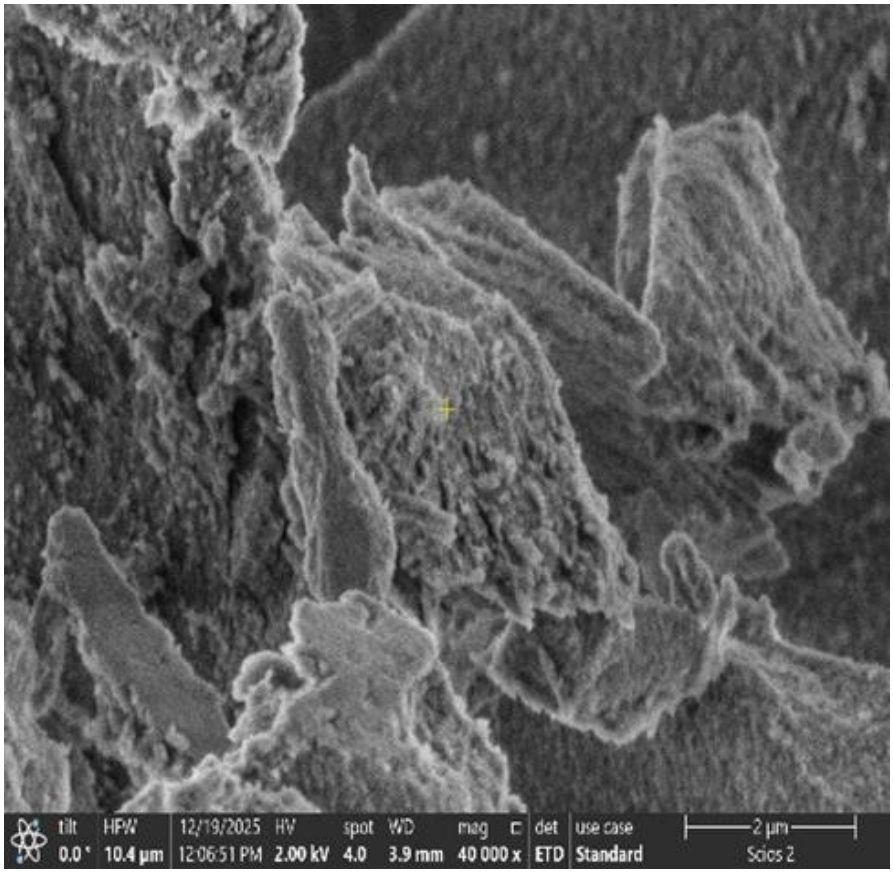
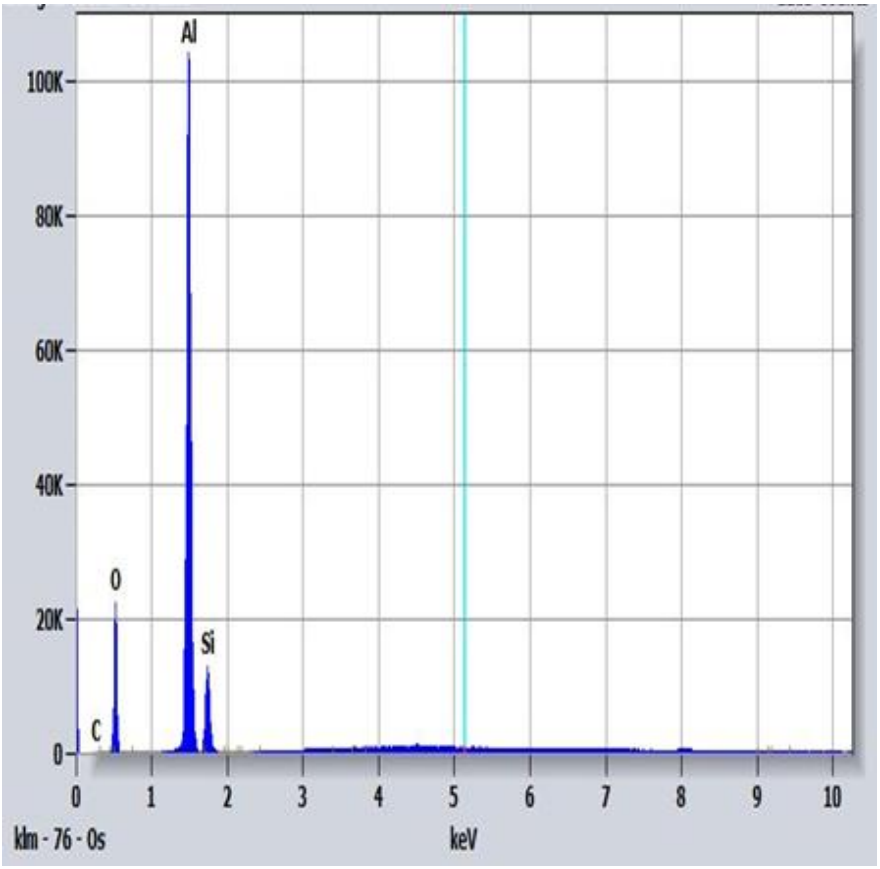


Fig. 8. TGA and dTG (insets) thermograms of industrial alumino-silica catalyst

The SEM images (figure 9) reveal irregular, porous agglomerates with rough surfaces and no well-defined crystalline features, typical of amorphous aluminosilicates. The particles are aggregated at the micrometer scale and exhibit a sponge-like morphology, consistent with mesoporosity. EDS mapping confirms a homogeneous distribution of Si, Al and O within the material.


tilt HFW 12/19/2025 HV spot WD mag det use case 2 µm
0.0 ° 10.4 µm 12:06:51 PM 2.00 kV 4.0 3.9 mm 40 000 x ETD Standard Scios 2


Al
O
Si
C
100K
80K
60K
40K
20K
0
0 1 2 3 4 5 6 7 8 9 10
keV
km - 76 - 0s

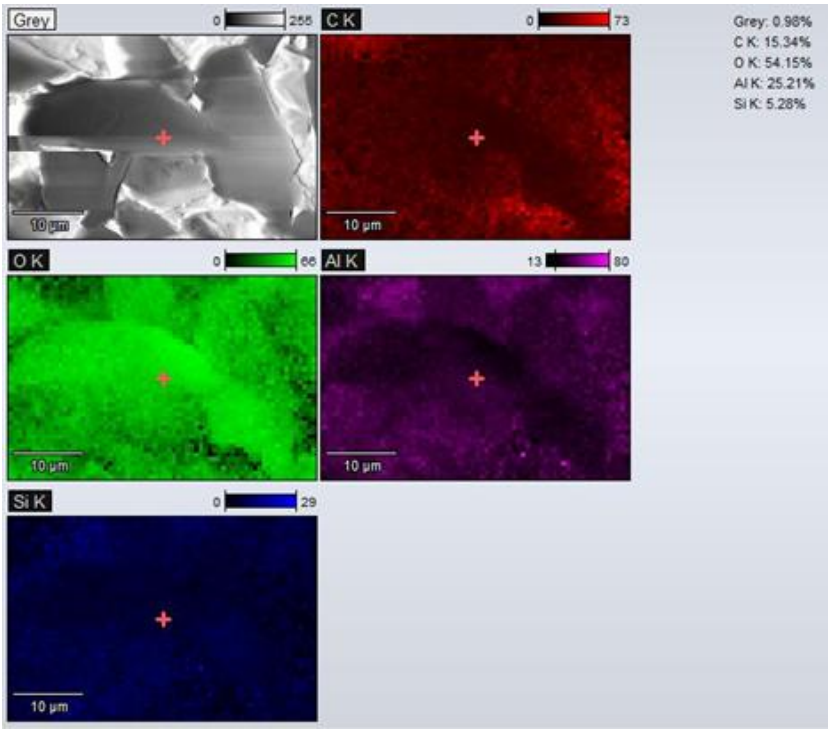


Fig. 9. SEM images for industrial oligomerization catalyst

The FT-IR spectrum (figure 10) shows the characteristic features of an amorphous aluminosilicate. Bands at ~418 cm-1 (Al-O), ~530 cm-1 (Si-O-Al), and ~1030 cm-1 (Si-O-Si / Si-O-Al) confirm the formation of a Si-Al framework. The band at 1633 cm-1 is attributed to adsorbed water, while the broad band at 3000-3800 cm-1 corresponds to surface hydroxyl groups. The absence of organic bands confirms the purity of the catalyst.

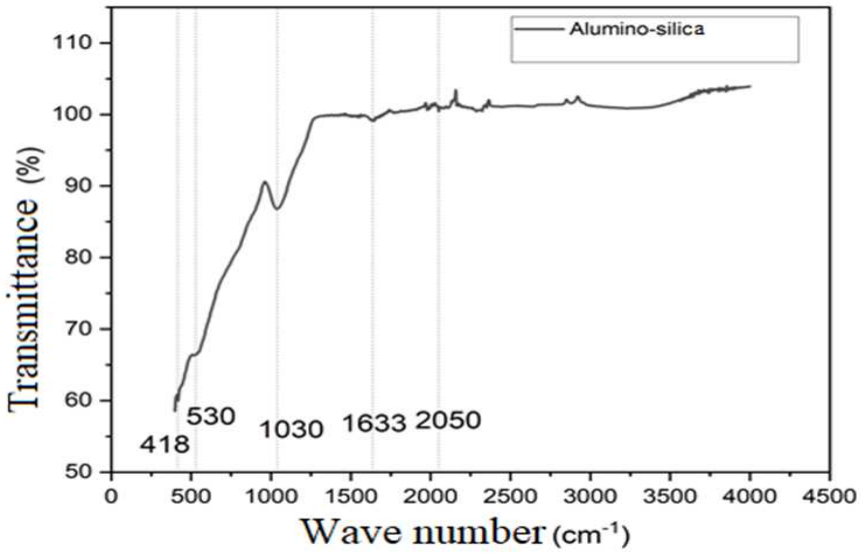


Fig. 10. FT-IR spectra of industrial oligomerization catalyst

The industrial catalyst is an amorphous mesoporous aluminosilicate with high surface area, well-developed porosity, and highly dispersed active species. These characteristics make it well-suited for olefin oligomerization, providing good accessibility, stability and catalytic performance.

A comparison between the synthesized Al-based mesoporous materials (Al-MCM-41, Al-MCM-48 and Al-SBA-15) and the industrial catalyst highlights significant differences in structural order, textural properties, and potential catalytic behavior. The synthesized materials exhibits well-defined mesostructural ordering, as confirmed by low-angle XRD, with Al-MCM-41 and Al-SBA-15 showing clear hexagon arrangements and Al-MCM-48 displaying a partially preserved cubic structure. In contrast, the industrial catalyst is full amorphous, lacking long-range structural order, as indicated by its XRD pattern. From a textural perspective, the synthesized materials possess highly uniform and well-organized mesoporosity, with a narrow pore size distributions and high specific surface areas, particularly in the case of Al-MCM-41 and Al-MCM-48. Al-SBA-15, although having a lower surface area, exhibits larger and more accessible pores, which can facilitate molecular diffusion. On the other hand, the industrial catalyst shows disordered mesoporosity with a broader pore size distribution, which may lead to less controlled diffusion but improved tolerance to pore blockage. Morphologically, SEM analysis reveals that the synthesized catalysts have more uniform particle sizes and controlled structures, whereas the industrial catalyst consists of irregular, agglomerated particles with a sponge-like texture, typical of amorphous aluminosilicates. In terms of thermal stability, all materials demonstrate good resistance to high temperatures, however, the industrial one exhibits simpler thermal behavior and high structural robustness, which is advantageous for long-term industrial operation.

Overall, the synthesized catalyst offers better structural control, higher uniformity and potentially enhanced selectivity, while industrial catalyst provides greater structural stability, robustness and practical applicability under industrial conditions. This highlights the trade-off between highly ordered mesostructures (academic materials) and amorphous but durable industrial catalysts.

All these findings underscore the importance of tailoring the synthesis route to the intended catalytic application. Aluminum-modified mesoporous materials that combine uniform acidity, accessible porosity, and robust structure are promising candidates for olefin oligomerization, ensuring high catalytic activity, selectivity, and durability under industrial operating conditions. For this reason, the following investigation has examined the impact of catalyst textural properties on the oligomerization process of propene.

3.6. Influence of catalyst type on propylene oligomerization

The conversion of propylene was investigated over the synthesized Al-MCM-41, Al-MCM-48, and Al-SBA-15 in a continuous fixed-bed reactor under identical operating conditions (5 barg, 1 g of catalyst), different reaction temperatures, and different reaction times. The pilot plant (Figure 11) is mainly composed of a propylene tank (99.5% purity supplied by Messer CANGas), a pressure reducer, a manual valve, two flow meters, one reactor (with a volume of the reaction zone of 5.8 cm^3), an electrical heater, a pressure indicator, a cooling water heat exchanger, a flash drum, a flow controller system, a temperature controller system.

The conversion of propylene on the industrial catalyst (alumino-silica) was investigated in the same fix-bed reactor under the same conditions as for the synthesized catalysts only the quantity of catalyst was changed to 6,5 g and volume of the reaction zone increased to 9,8 cm3.

Several series of tests were performed to determine the optimum operating conditions, and the most suitable results were obtained using 1g of catalyst, in the temperature range of 160 - 230°C, with a reaction time of 1-3 h, with flow rates between 75 and 150 ml/min of propylene. As mentioned before the quantity of industrial catalyst was 6,5 g.

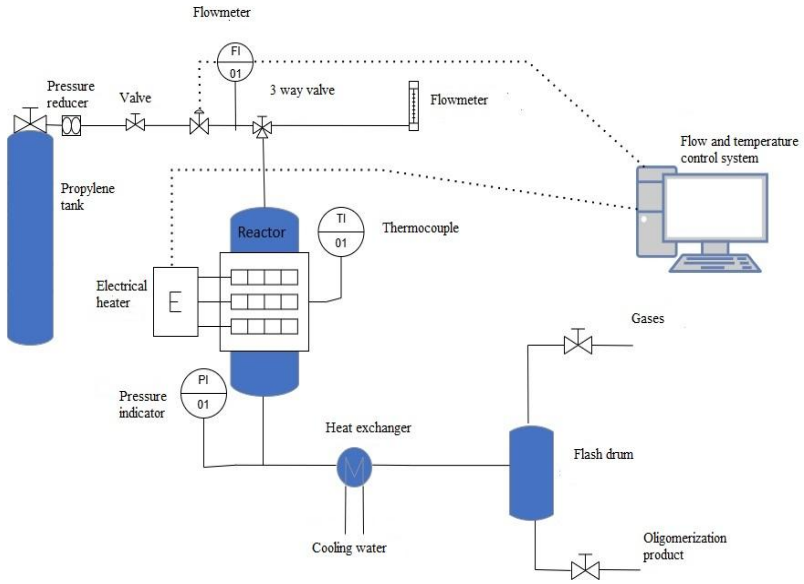


Fig. 11. Pilot plant for oligomerization of propylene

The catalytic performance was evaluated using the apparent rate of condensed liquid formation.

3.6.1.Influence of External Diffusion: Effect of Feed Flow Rate

To assess the possible influence of external mass transfer limitations, propylene oligomerization was performed at 200°C and 5 barg for 3 h using 1 g of catalyst for synthesized one and 6,5 g for industrial one, while varying the feed flow rate (75, 100 and 150 ml/min). Figure 12 shows the variation of total product vs. feed flow rate.

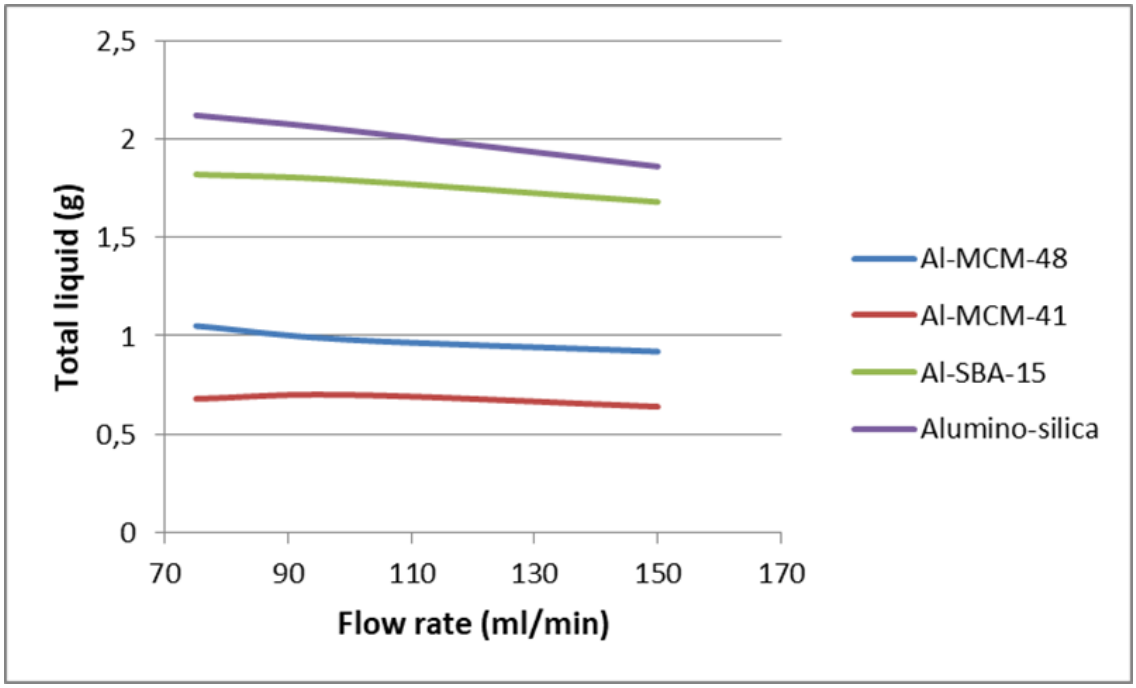


Fig. 12. Product variation with feed flow rate

For Al-MCM-48, the total mass of liquid product decreased with 12% when increasing the flow rate from 75 to 150 ml/min. For Al-MCM-41, the total mass of liquid product decreased with 6%, and for Al-SBA-15 with 8%. The industrial catalyst (alumino-silica) showed a decrease of 12% compared with Al-MCM-48. The decrease in total liquid production with increasing flow rate is systematic for all catalysts. Increasing the feed flow rate reduces the residence time of reactants in the catalytic bed. If strong external mass transfer limitations were present, increasing the flow rate would significantly enhance the reaction rate due to improved boundary layer transport. However, the experimental data show the opposite trend: productivity slightly decreases with increasing flow rate. The relative variation between 75 and 150 ml/min remains below 12% for all catalysts. Such modest dependence suggests that the reaction is not controlled by external film diffusion, the external mass transfer limitations are negligible, and the reaction proceeds predominantly in the kinetic regime.

At all flow rates, the activity order remains (Alumino-silica > Al-SBA-15 > Al-MCM-48 > Al-MCM-41) independently of flow rate, further indicating that intrinsic catalyst properties (pore structure, acid site accessibility, and diffusion inside the pore network) govern performance rather than external transport limitations. The larger mesopores of Al-SBA-15 likely facilitate faster evacuation of oligomers, reducing pore blockage and maintaining higher productivity. Al-MCM-48 benefits from its three-dimensional pore connectivity, while Al-MCM-41, characterized by one-dimensional channels, shows the lowest productivity.

Since external mass transfer limitations appear negligible, differences in catalytic performance are more plausibly associated with internal pore diffusion, product desorption limitations, and progressive pore blocking by heavy oligomers (C12+).

3.6.2.Total liquid formation as an apparent kinetic descriptor

The propylene oligomerization was performed at temperatures between 160°C and 230°C, with a duration of 3 hours for each experiment, at a flow of 100 ml/min propylene. The pressure didn't have an influence on the total product obtained, so the pressure was fixed at 5 barg.

Despite similar feed and pressure conditions, significant differences in liquid formation were observed between the four catalysts, indicating a strong influence of pore architecture on the overall reaction outcome. In particular Al-SBA-15 exhibits a pronounced increase in liquid yield compared to Al-MCM-48, Al-MCM-41 similar to industrial one.

The apparent rate of liquid formation was calculated according to equation (2) and used as a global kinetic proxy representative of gasoline-range hydrocarbon production.

$$r_{liq} = \frac{m_{liq}}{m_{cat} \times t} \ [g_{liq}/g_{cat} \cdot h] \quad (2)$$

where:

r_{liq} is the apparent rate of liquid formation,

m_{liq} is the mass of collected liquid (g),

m_{cat} is the mass of catalyst used in reaction (g),

t is the time of reaction.

Table 3. Apparent rate of liquid formation

Catalyst	T(°C)	r_{liq} ($g \cdot g_{cat}^{-1} \cdot h^{-1}$)
Al-MCM-48	160	0,1067
Al-MCM-48	180	0,1867
Al-MCM-48	200	0,3267
Al-MCM-48	230	0,4767
Al-MCM-41	160	0,05
Al-MCM-41	180	0,1233
Al-MCM-41	200	0,2333
Al-MCM-41	230	0,4167
Al-SBA-15	160	0,1533
Al-SBA-15	180	0,34
Al-SBA-15	200	0,5967
Al-SBA-15	230	1,0167
Alumino-silica	160	0,1635
Alumino-silica	180	0,3354
Alumino-silica	200	0,5296
Alumino-silica	230	0,8162

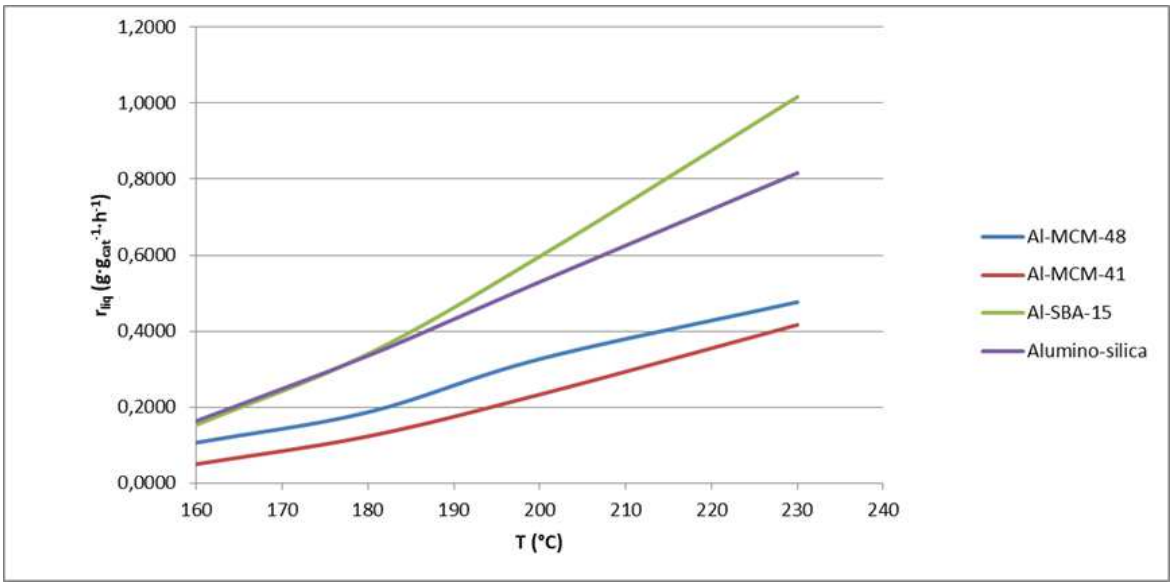


Fig. 13. Apparent liquid formation rate as function of temperature for Al-MCM-48, Al-MCM-41, Al-SBA-15 and industrial catalyst

Rates were calculated from the total condensed liquid collected during 3 h on stream at 5 barg and 100 ml/min propylene feed.

Figure 13 shows the temperature dependence of the apparent liquid formation rate for the four catalysts. At all temperatures, the activity order remained the same, with Al-SBA-15 having the highest activity similar to the industrial one. The differences between catalyst becomes more pronounced at higher temperatures. At 230°, Al-SBA-15 exhibits more than twice the apparent rate of Al-MCM-41. The superior performance of Al-SBA-15 can be attributed to larger pore diameter, improved accessibility of acid sites and lower susceptibility to pore blocking by heavy oligomers. Al-MCM-48 shows intermediate behavior, while Al-MCM-41 displays the lowest apparent rates. The industrial catalyst shows, at lower temperatures, similar rates compared with Al-SBA-15. At higher temperatures the apparent rate is lower with 20% than Al-MCM-48, but above Al-MCM-48 and Al-MCM-41.

The monotonic increase of apparent rate with temperature suggests that, under the investigated conditions, the reaction remains predominantly kinetically controlled within this temperature window. No decrease in activity at high temperature was observed, indicating that catalyst deactivation or excessive cracking does not dominate up to 230°C during the 3 h reaction period.

3.6.3.Apparent Arrhenius analysis

To further analyze the temperature dependence, an apparent Arrhenius treatment was applied using the condensed liquid formation rate (3):

$$\ln(r_{liq}) = \ln(A_{app}) - \frac{E_{a,app}}{R \times T} \quad (3)$$

where:

A_{app} is the pre-exponential factor,

$E_{a,\,app}$ is the apparent activation energy (kj/mol),

R is the gas constant equal to 8,314 J/mol · K,

T is the absolute temperature in K

Apparent Arrhenius plots of $\ln(r_{liq})$ versus 1/T are presented in **figure 14**.

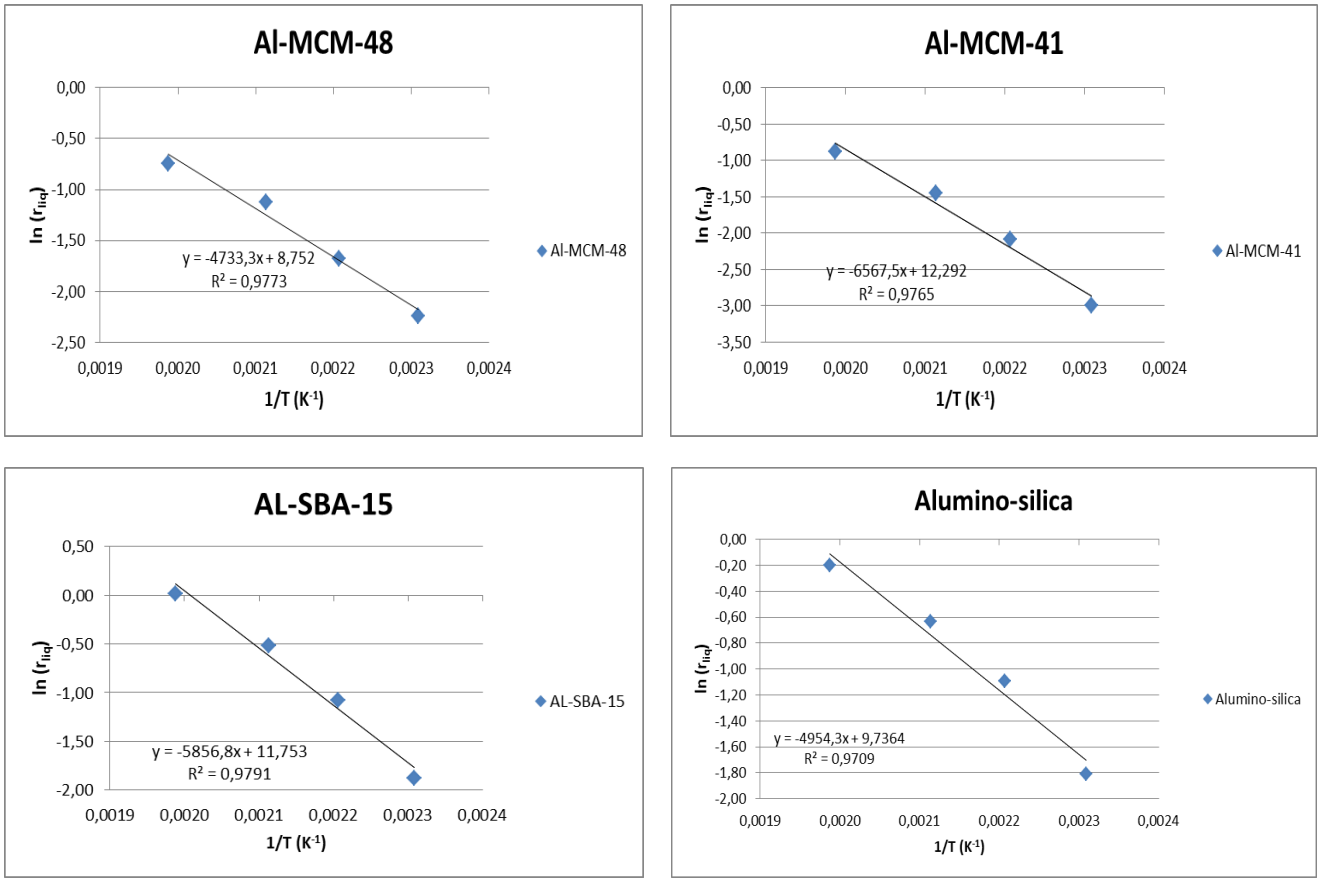


Fig. 14. Arrhenius representation of the apparent liquid formation kinetics over Al-MCM-48, Al-MCM-41, Al-SBA-15 and industrial catalyst

Linear trends were obtained over selected temperature intervals, allowing estimation of apparent activation energies and pre-exponential factors (**table 4**).

Table 4. Apparent Arrhenius parameters

Catalyst	$E_{a,\,app}$ (kJ/mol)	A_{app}	R^2
Al-MCM-48	39,4	6,23E+03	0,977
Al-MCM-41	54,6	2,18E+05	0,977
Al-SBA-15	48,7	1,27E+05	0,979
Alumino-silica	41,2	1,69E+04	0,971

The apparent activation energies ($E_{a,app}$) and pre-exponential factors (A_{app}) were obtained from liniear regression of $\ln(r_{liq})$ versus 1/T. Sincer r_{liq} represents the rate of condensed liquid formation under near-

complete propylene conversion, the extracted $E_{a,app}$ values reflect an apparent kinetic barrier that incorporates intrinsic reaction kinetics as well as transport and retention phenomena within the mesoporous network.

All catalyst show a clear Arrhenius-type dependence, with good linearity (R^2 = 0,97-0,98), indicating that the reaction rate increases exponentially with temperature in the investigated range. The apparent activation energies (39-55 kj/mol) fall within the typical range reported for acid-catalyzed olefin oligomerization over mesoporous aluminosilicates.

The Arrhenius analysis confirms that propylene oligomerization over mesoporous aluminosilicates is thermally activated within 160-230°C. The catalyst topology influences not only the absolute activity but also the temperature sensitivity of the apparent rate.

The combination of higher productivity and moderate apparent activation energy makes Al-SBA-15 the most efficient catalyst under the investigated conditions.

3.6.4.Time-on-stream behavior and catalyst stability

The evolution of liquid formation with time-on-stream at 200°C is shown in figure 15.

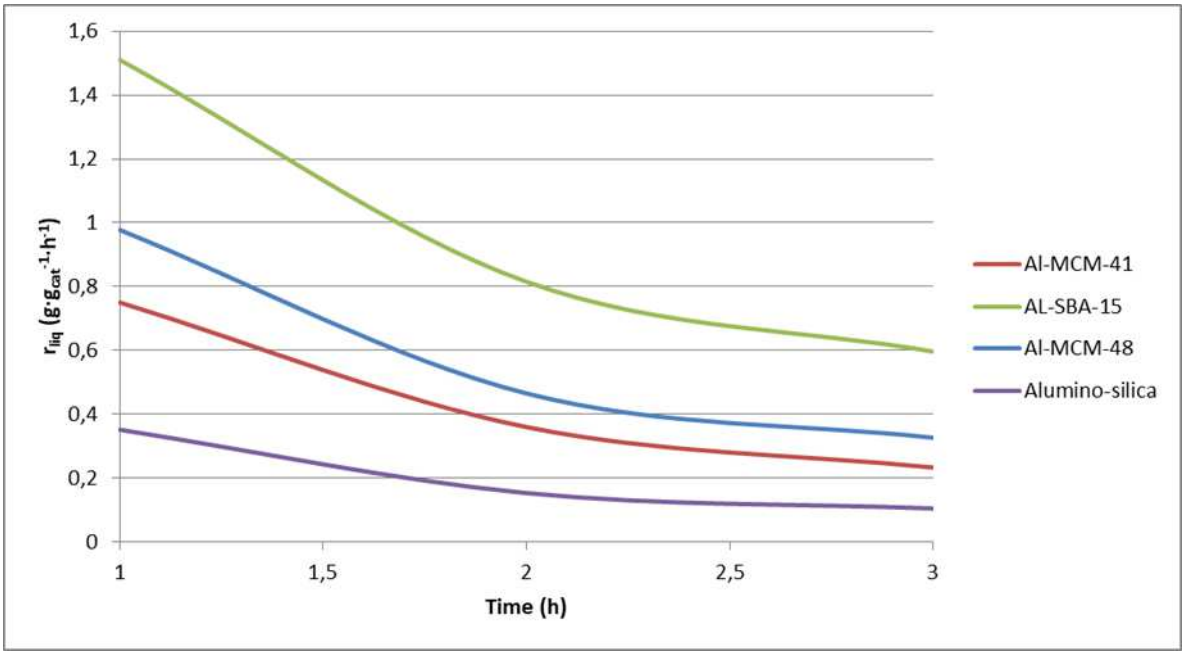


Fig. 15. Time-on-stream behavior at 200°C for Al-MCM-48, Al-MCM-41, Al-SBA-15 and industrial catalyst

The evolution of condensed liquid production (either cumulative mass or apparent rate) was monitored at 5 barg and constant propylene flow (100 ml/min).

All catalysts exhibit progressive deactivation (~65-70% activity loss). The most pronounced activity drop occurs during the first hour, indicating rapid initial deactivation. The deactivation likely originates from

formation of heavy oligomers (C12+), progressive pore blockage, coke precursor deposition on strong acid sites.

3.6.5. Product distribution

Detailed GC analysis was performed in order to estabilished the relative distribution of lumped products families – C6 oligomers, C9 oligomers, and heavier products (C10-C12+).

Figure 16 presents the products distribution for each catalyst type.

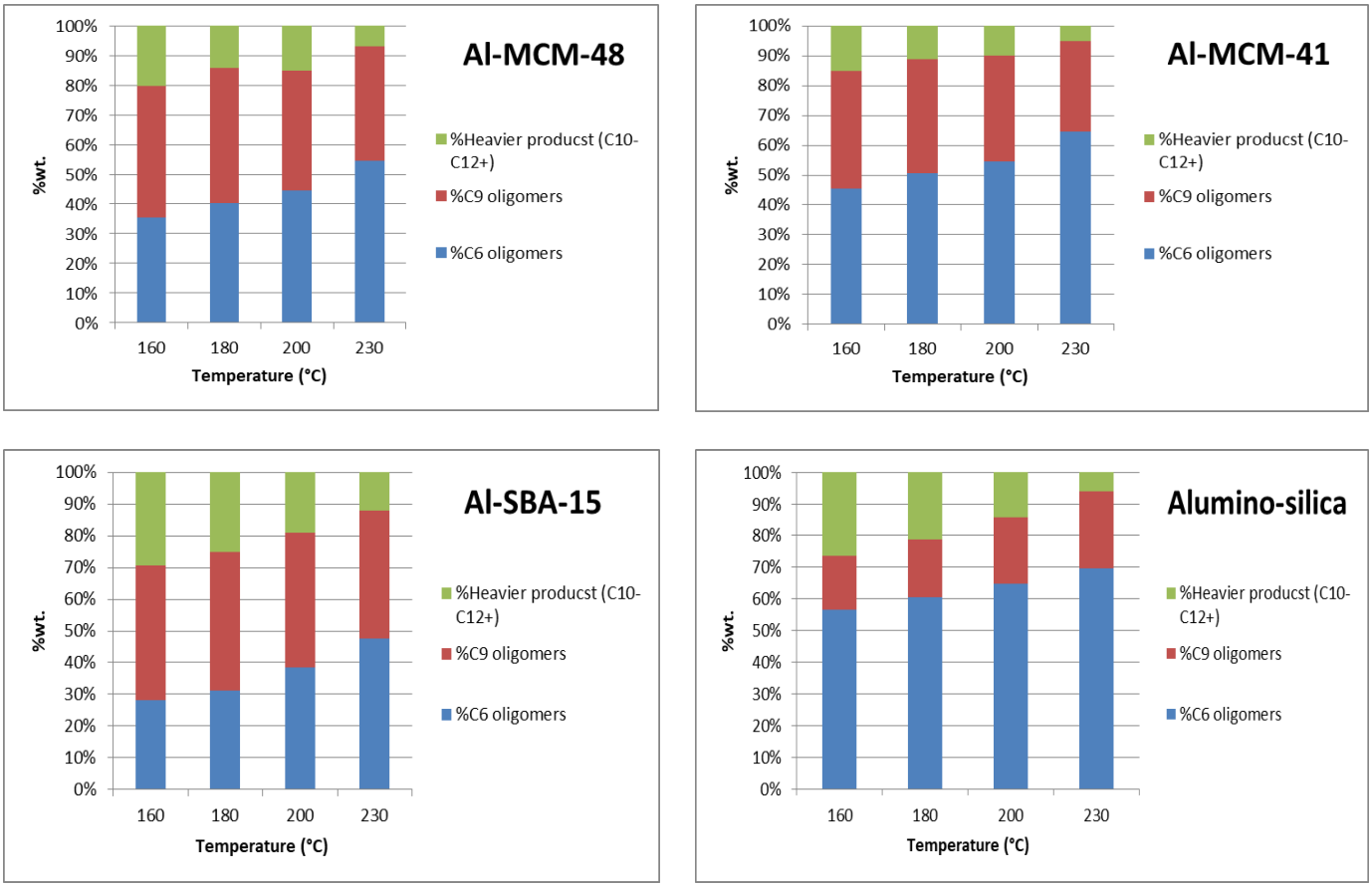


Fig. 16. Products distribution

Industrial catalyst shows the highest C6 selectivity (55-70%) and the C9 oligomers and heavier products are similar.

Al-MCM-41 shows highest C6 selectivity (45-65%) and lowest heavy fraction (5-15%). Increasing temperature shits distribution toward dimers, consistent with diffusion limitations in its 1D pore system.

Al-MCM-48 exhibits intermediate behavior, with balanced C6/C9 formation and moderate heavy product yield (7-20%), reflecting improved transport in the 3D pore network.

Al-SBA-15 maintains the highest heavy oligomer fraction (12-29%) at all temperatures and the lowest C6 selectivity. Large mesopores facilitate extended chain growth and reduce pore plugging.

For all catalysts, increasing temperature shifts selectivity toward C6 and decreases heavy products, indicating enhanced chain termination and β-scission at higher temperatures.

4. Conclusions

This work demonstrated that the incorporation of aluminum into the structure of mesoporous silica materials has a significant impact on their structural, textural, and thermal properties. MCM-41, characterized by a well-ordered hexagonal structure, was the most sensitive to the aluminum incorporation, which preserved the structural regularity, surface area, and pore accessibility. Al-MCM-48 exhibited higher crystallinity, uniform morphology, and improved thermal stability. The incorporation of aluminum into the ordered structure of SBA-15 resulted in a more uniform distribution of Al species within the framework, better preserving pore accessibility and stability.

Propylene oligomerization over mesoporous aluminosilicates is strongly governed by pore architecture. External mass transfer limitations were negligible under the investigated conditions, and the reaction exhibited clear Arrhenius behavior within 160-230°C, with apparent activation energies between 39 and 55 kj/mol.

Catalytic performance consistently followed the order: Alumino-silica / Al-SBA-15 > Al-MCM-48 > Al-MCM-41.

Al-SBA-15 demonstrated the highest productivity, superior heavy oligomer (C10-C12+) selectivity, and improved resistance to deactivation compared with the industrial catalyst, attributed to its larger mesopores and enhanced product diffusion. Al-MCM-41, characterized by one-dimensional channels, favored lighter oligomers and showed faster deactivation due to strong diffusion constrains and pore blocking. Al-MCM-48 exhibited intermediate behavior, reflecting the benefits of its three-dimensional pore connectivity.

Overall, the results confirm that pore size and connectivity are decisive parameters controlling acitivity, selectivity and stability in propylene oligomerization over mesoporous aluminosilicates.

5. Conflict of interest

The author(s) declared no potential conflicts of interest with respect to the research, authorship, and/or publication of this article.

6. Fundings

This research received no external fundings.

7. Author contributions

Conceptualization, D.M., D.L.C., and M.P.; methodology, D.M.; software, D.M., and S.M.; validation, D.M., D.L.C., and M.P.; formal analysis, D.M. and S.M.; investigation, D.M.; resources, D.M. and D.L.C.; data curation, D.M.; writing—original draft preparation, M.P.; writing—review and editing, M.P., D.M. and D.L.C.; visualization, M.P., D.L.C. and S.M.; supervision, D.L.C and S.M.; All authors have read and agreed to the published version of the manuscript.

References

1. Eimer, G.; Pierella, L.; Monti, G.; Anunziata, O. Synthesis and characterization of Al-MCM-41 and Al-MCM-48. Catalysis Letters 2002, 78, 1-4. https://doi.org/10.1023/A:1014924332500
2. Kumaran, G.; Garg, S.; Soni, K.; Kumar, M.; Gupta, J.; Sharma, L.; Rao, K.; Dhar, G. Synthesis and characterization of acidic properties of Al-SBA-15 materials with varying Si/Al ratios. Materials 2008, 114, 103–109. https://doi.org/10.1016/j.micromeso.2007.12.021
3. Aldosari, O.; Alhumaimess, M.; Betiha, M.; Ahmed, E.; Alhaidari, L.; Altwala, A.; Hassan, H. Characterization and Catalytic Performance of Al-SBA-15 Catalyst Fabricated Using Ionic Liquids with High Aluminum Content. Catalysts 2023, 13, 1395-1410. https://doi.org/10.3390/catal13111395
4. Kosslicka, H.; Lischkeb, G.; Parlitza, B.; Storekc, W.; Frickea, R.; Acidity and active sites of Al-MCM-41. Applied Catalysis A: General 1999, 184, 49-60. https://doi.org/10.1016/S0926-860X(99)00078-2
5. Abdrassilova, A.; Vassilina, G.; Abdildina, K.; Briones, L.; Peral, A.; Escola, J.M. The notable features of mesoporous aluminosilicates as catalytic supports for hydrodearomatization and hydrodesulfurization of fuels. Microporous and Mesoporous Materials 2025, 384, 113457-113476. https://doi.org/10.1016/j.micromeso.2024.113457
6. W. Li, D. Zhao, An overview of the synthesis of ordered mesoporous material. Chem. Commun **49**, 943 (2013). https://doi.org/10.1039/C2CC36964H
7. Á. Szegedi, M. Popova, V. Mavrodica, M. Urbán, I. Kiricsi, C. Minchev, Synthesis and characterization of Ni-MCM-41 materials with spherical morphology and their catalytic activity in toluene hydrogenation. Microporous and Mesoporous Materials **99**, 149 (2007). DOI:10.1016/j.micromeso.2006.07.040
8. Y. Shu, Y. Shao, X. Wei, X. Wang, Q. Sun, Q. Zhang, L. Li, Synthesis and characterization of Ni-MCM-41 for methyl blue adsorption. Microporous and Mesoporous Materials **214**, 88 (2015). DOI:10.1016/j.micromeso.2015.05.006
9. S. Bhattacharyya, G. Lelong, M.L. Saboungi, Recent progress in the synthesis and selected applications of MCM-41: a short review. Journal of Experimental Nanoscience **1**(3), 375 (2006). https://doi.org/10.1080/17458080600812757
10. V. Meynen, P. Cool, E.F. Vansant, Verified syntheses of mesoporous materials. Microporous and Mesoporous Materials **125**, 170 (2009). https://doi.org/10.1016/j.micromeso.2009.03.046
11. Z.A. AlOthman, A Review: Fundamental Aspects of Silicate Mesoporous Materials. Materials **5**, 2874 (2012) https://doi.org/10.3390/ma5122874

12. Soltani, S.; Khanian, N.; Rashidc, U.; Yaw Choong, T. Fundamentals and recent progress relating to the fabrication, functionalization and characterization of mesostructured materials using diverse synthetic methodologies. RSC Adv., 2020, 10, 16431-16456. https://doi.org/10.1039/d0ra00440e

13. Locus, R.; Verboekend, D.; Zhong, R.; Houthoofd, K.; Jaumann, T.; Oswald, S.; Giebeler, L.; Baron, G.; Sels. B. Enhanced Acidity and Accessibility in Al-MCM-41 through Aluminum Activation. Chem. Mater. 2016, 28, 21, 7731-7743. https://doi.org/10.1021/acs.chemmater.6b02874

14. A. Ahmad, M.H. Razali, K.A.M. Amir, Review of Metal Supported on Mesoporous MCM-41 as Catalyst for CNTs Growth. IOP Conference Series: Material Science and Engineering **440** (2018). doi:10.1088/1757-899X/440/1/012025

15. A. Corma, From Microporous to Mesoporous Molecular Sieve Materials and Their Use in Catalysis. Chemical Reviews **97**, 2373 (1997). https://doi.org/10.1021/cr960406n

16. Yılmaz, M.; Ozdemir, O.; Piskin, S. Synthesis and characterization of MCM-41 with different methods and adsorption of Sr2+ on MCM-41. Res Chem Intermed 2013, 41, 199–211. https://doi.org/10.1007/s11164-013-1182-4

17. Jana, S.; Takahashi, H.; Nakamura, M.; Kaneko, M.; Nishida, R.; Shimizu, H.; Kugita, T.; Namba, S. Aluminum incorporation in mesoporous MCM-41 molecular sieves and their catalytic performance in acid-catalyzed reactions. Applied Catalysis A: General 2003, 245, 33-41. https://doi.org/10.1016/S0926-860X(02)00616-6

18. Prabhu, A.; Sudha, V.; Pachamuthu, M.; Sundaravel, B.; Bellucci, S. Ultrasonic Synthesis of Al-SBA-15 Nanoporous Catalyst for t-Butylation of Ethylbenzene. Journal of Nanomaterials 2022, 2022, 1-10. https://doi.org/10.1155/2022/2512223

19. M.-H. Kwon, H.-J. Chae, M.B. Park, Oligomerization of 1-hexene over designed SBA-15 acid catalysts. Journal of Industrial and Engineering Chemistry **65**, 397 (2018). DOI :10.1016/j.jiec.2018.05.012

20. D.E. Romero, M. Rigutto, E.J.M. Hensen, Influence of the size. order. and topology of mesopores in bifunctional Pd-containing acidic SBA-15 and M41S catalysts for n-hexadecane hydrocracking. Fuel Processing Technology **232**, 107259 (2022), https://doi.org/10.1016/j.fuproc.2022.107259

21. K.M. Parida, S.K. Dash, D. Rath, Synthesis of mesoporous silica. In Comprehensive Guide for Mesoporous Materials. Properties and Development, Editor Aliofkhazraei Mahmood, Publisher Nova, New York, 2015, Volume 3, 43-65.

22. M. Tanaka, A. Itadani, Y. Kuroda, M. Iwamoto, Effect of Pore Size and Nickel Content of Ni-MCM-41 on Catalytic Activity for Ethene Dimerization and Local Structures of Nickel Ions, J. Phys. Chem. C **116**, 5664 (2012). DOI: 10.1021/jp2103066

23. S. M. Zakir, P. Taba, N. La. Nafie, I. Indriani, Synthesis of MCM-41 Silica Mesoporous Modified with Zn Metal, Journal Kimia Sains dan Aplikasi **25**(8), 286 (2022). https://doi.org/10.14710/jksa.25.8.286-291

24. P. Trongjitraksa, A. Jantharasuk, W. Jareewatchara, Y. Klinthongchai, B. Jongsomjit, P. Praserthdam, Enhancement of the themal stability for MCM-48 with incorporation of different metals, Microporous and Mesoporous Materials **354**, 112556, (2023)**.** https://doi.org/10.1016/j.micromeso.2023.112556.

25. P. Sriratchatchawan, S. Eaimsumang, S.M. Smith, S. Boonyuen, C. Ngamcharussrivichai, A. Luengnaruemitchai, Acidic properties of propyl sulfonic acid functionalized SBA-15 catalysts for acetylation of glycerol, Heliyon **10** (24), e41044 (2024). doi: 10.1016/j.heliyon.2024.e41044

26. P. Tosuwan, S.-Y. Chen, H. Tateno, T. Mochizuki, A. Luengnaruemitchai, An aluminum-grafted SBA-15-catalyzed conversion of glucose to 5- hydroxymethylfurfural, Catal. Commun. **170**, 106488 (2022), https://doi.org/10.1016/j.catcom.2022.106488

27. D. Matei, M. Postelnicu, S. Mihai, D.-L. Cursaru, Influence of the Synthesis Method on the Textural and Morphological Characteristics of Ni-Based Mesoporous Molecular Sieves, Materials **18**(5), 1012 (2025), https://doi.org/10.3390/ma18051012